Performance of the IBIS Compton mode

Alberto Segreto

Alberto Segreto, "Performance of the IBIS Compton mode," Proc. SPIE 5488, UV and Gamma-Ray Space Telescope Systems, (11 October 2004); doi: 10.1117/12.554933

SPIE.

Event: SPIE Astronomical Telescopes + Instrumentation, 2004, Glasgow, United Kingdom

PERFORMANCE OF THE IBIS COMPTON MODE

A. Segreto

[a]IASF/CNR, Via Ugo La Malfa 153, Palermo, Italy

ABSTRACT

The IBIS instrument launched on board the ESA INTEGRAL observatory on October 2002 is a coded mask telescope composed by two position sensitive detection planes, one with 16384 Cadmium Telluride pixels (ISGRI) and the other with 4096 Caesium Iodide pixels (PICsIT).

Events detected in coincidence in the two detector layers are flagged as generated by Compton scattered photons and can be then processed and filtered using the Compton kinematic equations. The analysis of these data is, however, quite complex, mainly due to the presence of a great number of fake events generated by random coincidences between uncorrelated ISGRI and PICsIT events; if this component is not subtracted with great accuracy, false source detections can be produced.

In this work, we present the performance (spectral and imaging) obtainable from the IBIS Compton data, by analyzing ground calibration acquisitions. We also analyze the IBIS Compton flight data relative to the Crab observation, to determine its scientific capabilities.

Keywords: IBIS, ISGRI, Compton, INTEGRAL

1. INTRODUCTION

The IBIS instrument, launched on board the ESA INTEGRAL observatory on October 2002, is a coded mask telescope, operating in the range 15 keV - 10 MeV, composed by two position sensitive detection planes: ISGRI (CdTe) and PICsIT (CsI).

Events detected in coincidence between the two layers are flagged as Compton data. Here, we present some results obtained from the analysis of the these data acquired during the INTEGRAL payload ground calibrations, in order to show which are the spectral and imaging performances (angular resolution and localization accuracy) obtainable from the application of the Compton kinematics.

After verification of the in-flight performances of the Compton data, by analyzing the data associated to the IBIS on-board Calibration Unit, we then analyze data relative to the Crab pointing to establish which are the astrophysical capabilities obtainable from the use of these IBIS data.

2. IBIS DESCRIPTION

The IBIS[1] instrument, is a coded aperture telescope, consisting of two position sensitive detector planes: ISGRI[2] (INTEGRAL Soft Gamma-Ray Imager) and PICsIT[3] (Pixelated Imaging Cesium Iodide Telescope). ISGRI consists of 16384 (arranged in a 128 x 128 matrix) CdTe semiconductor detectors. Each detector is 2 mm thick and 4 x 4 mm in geometrical area. ISGRI nominal energy range is 15 keV - 1 MeV, with an energy resolution of 8% FWHM at 100 keV. The PICsIT layer is located 10 cm below ISGRI, and consists of 4096 (arranged in a 64 x 64 matrix) 3 cm long CsI(Tl) crystals with a square area of 8.4 x 8.4 mm and photodiode readout; its nominal working energy range is 175 keV - 6.8 MeV. The two detectors are shielded by an active anticoincidence system made of 20 mm thick BGO crystals with PMT readout.

A coded mask, made of 16 mm thick tungsten elements, is located 3.2 m above the detector planes. It is made up of 95 x 95 individual square cells, of size 11.2 x 11.2 mm each, forming a coded MURA pattern. The angular resolution achieved which such a configuration is 12 arcmin. The IBIS Fully Coded Field of View is 9.2° and the Partially Coded Field of View, up to zero response, is 29°.

Further author information: (Send correspondence to A.S.)
A.S.: E-mail: segreto@pa.iasf.cnr.it

UV and Gamma-Ray Space Telescope Systems, edited by
Günther Hasinger, Martin J. L. Turner, Proceedings of SPIE Vol. 5488
(SPIE, Bellingham, WA, 2004) · 0277-786X/04/$15 · doi: 10.1117/12.554933

3. THE COMPTON DATA

An ISGRI event and a PICsIT event detected within a coincidence time window ($\Delta T_{\rm C}$) are considered correlated and generated by Compton scattered photons.[4] These correlated events are associated and transmitted separately from the other IBIS data.

The temporal correlation between ISGRI and PICsIT events can only be tested by the IBIS on-board software, to which the full timing information generated by the two detector layers is available. In fact, in order to reduce the telemetry bit rate, the time resolution of the instruments, which is $\simeq 0.2348$ μsec, is degraded to 61 μsec when the events are transmitted. The Compton coincidence time window is set to a value much wider than the instrumental time resolution to take into account that ISGRI events are generated with a jitter of the order of few μs with respect to the real photon interaction times.[2]

Since the average electronic delay of ISGRI events with respect to correlated PICsIT events is compensated by an adjustable offset, the coincidence time window is applied in a symmetric way, that is an ISGRI and a PICsIT event whose time difference is within $\pm\Delta T_{\rm C}$ are considered correlated. In the nominal configuration the coincidence time window is set to 2μs.

Due to the quite large value of the correlation time window and to the high background count rate of the detectors, a large amount of random coincidences between uncorrelated ISGRI and PICsIT events is also generated. The expected rate of random coincidences can be obtained, with a good approximation, from $R = 2\cdot \Delta T_{\rm C}\cdot R_{\rm I}\cdot R_{\rm P}$, where $R_{\rm I}$ and $R_{\rm P}$ are the count rate of the ISGRI and PICsIT single events. A more precise way to compute the number of random coincidences is described in Ref. 5.

3.1. Compton energy spectra

The energy spectra of Compton data are obtained summing up ISGRI and PICsIT energy deposits of the correlated events. In the analysis of these spectra it is important to consider that to obtain the source spectrum it is necessary to subtract, together with the standard background, also the contribution of the random coincidences. Random coincidences, in fact, depend on the source count rate and are not removed by the application of usual background subtraction methods. The spectrum of the random coincidences can be obtained summing the energy of randomly associated ISGRI and PICsIT 'single' events, and then normalized to the expected rate.

As example, the left panel of Fig. 1 shows the Compton spectrum obtained, after usual background subtraction, from an acquisition of a ^{241}Am source, compared with the spectrum formed by the random coincidences (continuous line); as expected, because the ^{241}Am source do not generate any photon at so high energy, the two spectra are consistent over the whole energy range.

This example clearly show that, without the subtraction of the correct amount of random coincidences, meaningless high energy spectra could be generated from Compton data. The method that can be used to evaluate and subtract random coincidences with great accuracy is described in more details in Ref. 5, 6.

The right panel of Fig. 1 shows the background subtracted Compton spectrum obtained from an acquisition with an illuminating ^{22}Na source before and after the subtraction of random coincidences. Note that, together with the two gaussian lines (at 511 keV and 1274 keV) correspondent to photons whose total energy has been deposited in the detectors (a Compton scattering plus a photoelectric absorption), low energy tails below these line energies are present. The tails indicate that a quite high fraction of Compton events, are generated by photons that escape after two scatterings. For these events the total photon energy is underestimated.

The energy resolution (FWHM) measured from the reconstructed ^{22}Na spectrum is 15% at 511 keV and 7.5% at 1275 keV.

3.2. The Compton scattering angle

For each couple of events detected in coincidence in the two IBIS layers we can compute the scattering angle ($\Phi_{\rm C}$) using the following equation derived from the Compton kinematics:

$$cos(\Phi_{\rm C}) = 1 - \frac{E_1 \cdot m_{\rm e}c^2}{E_2 \cdot (E_1 + E_2)} \qquad (1)$$

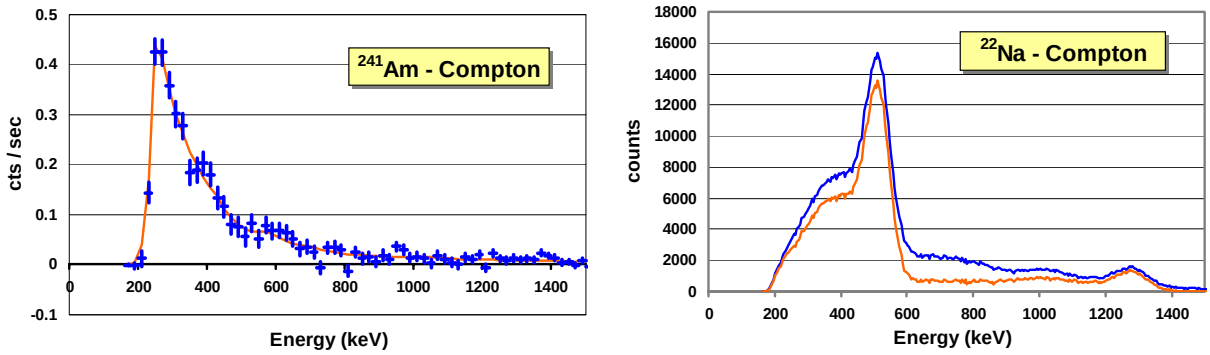

Figure 1. In the left panel, the background subtracted Compton spectrum obtained from an ^{241}Am acquisition (crosses), compared with the spectrum of random coincidences (continuous line) is shown. In the right panel the background subtracted ^{22}Na 'Compton single' spectra obtained before (upper curve) and after (lower curve) the subtraction of random coincidences is plotted.

where $m_e c^2$ is the electron rest mass energy (511 keV), E_1 the energy deposited in the first photon interaction and E_2 the energy deposited in the second interaction. Note that, we obtain the correct scattering angle from Eq. 1 only when the photon releases its whole energy in the two interactions, that is when the Compton scattered photon is totally absorbed. If in its 2nd interaction the photon is scattered again and escape from the instrument, the angle obtained from Eq. 1 will be higher than the true scattering angle.

Due to the limited time resolution with respect to the time of flight between the two detector layers (distance of the layers 10 cm), it is not possible to determine which layer has been hit first, and it is then not possible to separate the down-scattered (first interaction on ISGRI) from the up-scattered (first interaction on PICsIT) events; Eq. 1 then gives, for each Compton event, two possible scattering angles.

3.3. The ARM distribution

When the position of the source is known, we can compute the Compton scattering angle also from the geometrical coordinates of the two interaction points. This angle is called the 'geometric angle' (Φ_G) and, again, two possible values depending whether the first interaction is assumed to be on ISGRI or on PICsIT are obtained.

When the source is at infinite distance and in on-axis position, denoting with H the distance between the two detector layers and with D the distance between the two interaction points, the geometric angle can be obtained, assuming a down-scattered photon, from

$$cos(\Phi_G) = \frac{H}{D} \tag{2}$$

or, assuming an up-scattered photon, from

$$cos(\pi - \Phi_G) = \frac{H}{D} \tag{3}$$

Of course, when the source is in off-axis position or at finite distance (as during the on-ground calibration), formula 2 and 3 should be replaced by the correct ones.

According to the angle definition, Compton scattered photons arriving from the source direction should have $\Phi_C = \Phi_G$, however the measured values will be different due to the limited energy and spatial resolution of the detectors. The correlation between the Φ_C and Φ_G angles for Compton events of a ^{22}Na acquisition performed during the ground IBIS calibration is shown in the left panel of Fig. 2. For both angles, we assumed the down-scattering condition and selected the events in the 511 keV line. The correlation between these two angles is clearly visible along the $\Phi_C = \Phi_G$ line.

For Compton telescopes, the histogram of the difference between the Φ_C and Φ_G angles is known as the Angular Resolution Measure (ARM) distribution.[7] In the ARM distributions ($ARM = \Phi_C - \Phi_G$), the Compton

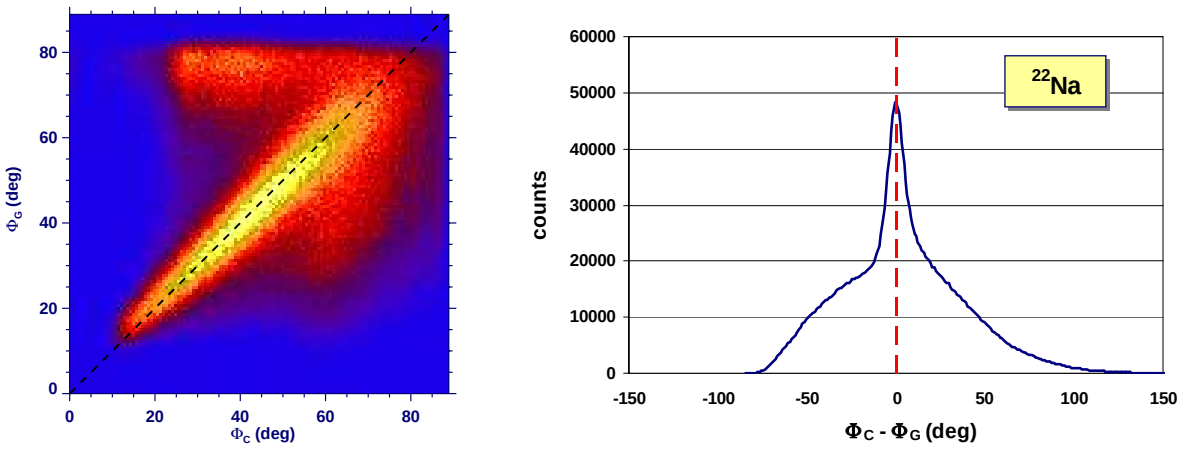

Figure 2. In the left panel, the 2D histogram diagram shows the correlation between the Φ_C and Φ_G angles for the 511 keV photons generated by a ^{22}Na calibration source. In the right panel, the correspondent ARM distribution is shown.

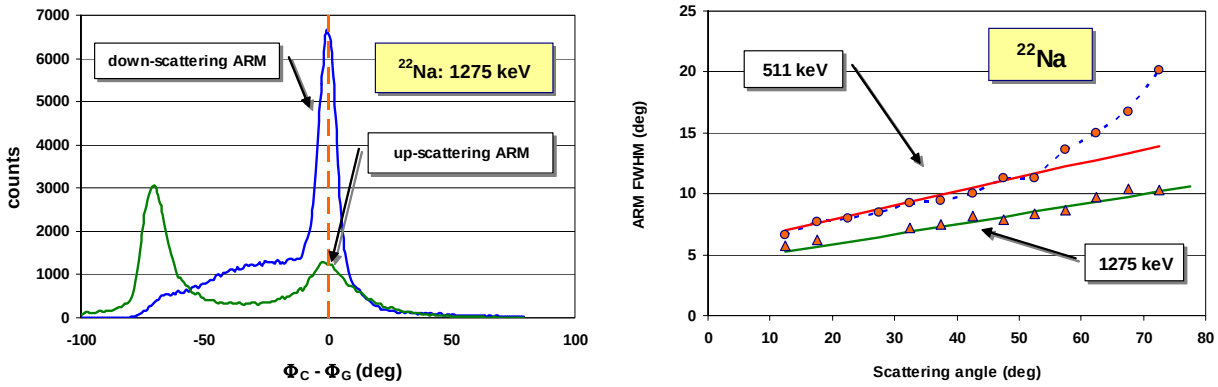

Figure 3. On the left panel the up-scattering and down-scattering ARM distributions from a ^{22}Na acquisition, obtained selecting only the events in the 1275 keV line are shown. The FWHM of the lines are 8.1° for down-scattering and 13° for the up-scattering distribution. As evident from line comparison, the up-scattered events constitute only $\sim 20\%$ of the total number of 1275 keV detected Compton events. In the left panel the angular resolution as function of the scattering angle, measured at 511 keV and 1275 keV is shown . The lines shown in the diagram are defined as $FWHM(\Phi_S) = 5.6^\circ + 0.115 \cdot \Phi_S$ for the 511 keV line and $FWHM(\Phi_S) = 4.2^\circ + 0.08 \cdot \Phi_S$ for the 1275 keV line.

scattered photons originating from the source direction can be easily identified because they form a narrow line at the origin, on top of a much broader distribution due to background events. The angular resolution of a Compton telescope is usually defined as the FWHM of its ARM distribution, and depends of course on the detector accuracy in reconstructing the energy and the interaction position of the two events.

The right panel of Fig. 2 shows the ARM distribution obtained from the ^{22}Na acquisition. Note that the line at the origin appear asymmetric with a tail on the right side. This tail is due to events generated by multiple scattered photons. For these events the Compton scattering angle is overestimated due to the partial deposition of the photon energy in the detectors.

Depending wether the Φ_C and Φ_G angles are computed using the down-scattering or up-scattering equations two different ARM distributions can be obtained from the same data set. Fig. 3 shows the up and down scattering ARM distributions obtained from the ^{22}Na acquisition selecting the Compton events whose reconstructed energy is in the 1275 keV line. Note that the events outside the lines at the origin are in part due to background events and in part due to source events with the scattering direction opposite to the one assumed. The FWHM of the

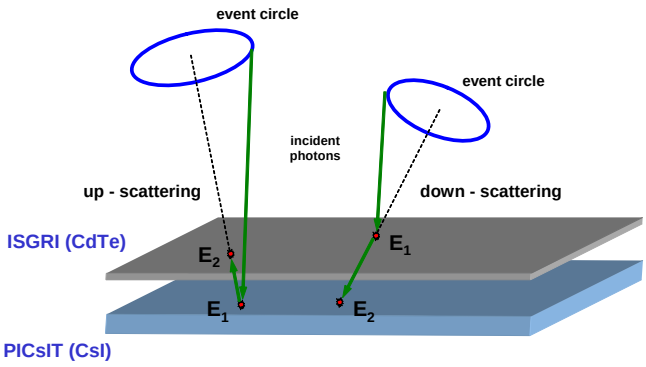

Figure 4. Definition of Compton cones and event circles

lines at the origin are $\sim 8°$ in the down-scattering and $\sim 13°$ in the up-scattering ARM distribution.

Since in the down-scattering ARM distribution the up-scattered photons do not contribute to the line at the origin and viceversa, the ratio between down-scattered and up-scattered photons can be derived simply from the ratio between the number of events in the two lines. As evident, $\sim 80\%$ of the detected Compton events at 1275 keV (full energy deposits) are generated by down-scattered photons.

As already evident from the from the 2D histogram shown in Fig. 2, the region of correlation along the $\Phi_C = \Phi_G$ line, that is the width of the line in the ARM distribution, become broader with increasing scattering angles. In the right panel of Fig. 3, the FWHM of the down-scattering ARM distribution is plotted for the two ^{22}Na line energies, as function of the scattering angle defined as $\Phi_S = (\Phi_C + \Phi_G)/2$.

4. COMPTON IMAGING

The energy deposits and the interaction positions observed in the two IBIS detector planes, allow to determine the Compton scattering angles and to confine the incident photon directions on a cone surface; the intersection of this cone with a plane is usually referred to as an 'event circle' (Fig. 4). When the source is at infinite distance, the simplest method to generate a sky image is to overlap the projection in the sky of the event circles associated with the Compton events (back-projection).

When the source is at finite distance, like during ground calibrations, its 3-D coordinates can be obtained by the intersection of the Compton cone surfaces. This three dimensional problem can handled in a easier way by scanning the 3-D space with planes placed at different distances from the coordinate origin or with concentric spheres whose center is in the coordinate origin. In each of these planes or spheres an image can be obtained summing the 'event circles' generated by the intersection of the 'Compton cones' with the considered surface. The source will be best imaged in the plane or sphere that contains the source location.

Of course, when a sphere is used to generate a Compton image, this must be successively projected in a plane for visualization. This can be done in several ways, but we find convenient to represent the imaging sphere in a plane using the Azimuthal Equidistant Projection. This projection is a polar diagram where the angle is the azimuth of the point of the sphere and the radius is its zenit angle (θ). Concentric circles in the image then represent all the points of the sphere having the same off-axis angle.

The main advantage of the Azimuthal Equidistant Projection is that it is possible to represent a whole hemisphere in a single map, with no angular distortion at all in the radial directions and with an acceptable distortion in the other directions up to high off-axis angles. In order to maintain the same areal density of events measured on the sphere also in the projected image, from simple geometrical considerations, it can be shown that the sky image should be divided by $sin(\theta)/\theta$. In this case, a spherically isotropic distribution of event circles would generate a flat uniform sky image. Any deviation from a flat distribution in the reconstructed skymap can the be attributed to true anisotropy in the spatial distribution of the directions of the detected photons.

Depending whether the 'down-scattering' or the 'up-scattering' Compton equations are used to generate the event circles, we obtain two different skymaps from the same dataset; however, as seen before, the up-scattered events are less numerous and have a worst angular resolution, so the skymaps reconstructed using the up-scattering equations are of much poorer quality with respect to skymap obtainable from the down-scattering equations.

4.1. Field of view

With image reconstruction methods based on the Compton kinematics it is possible to reconstruct skymaps having a very large field of view. To give an example of this capability, we analyze the Compton data obtained, during the payload calibrations, by illuminating IBIS with a ^{24}Na radioactive source placed at an off-axis angle of $\sim 40°$, along the line of sight connecting the IBIS detector plane with the coded mask of the SPI instrument (another imaging detector on-board INTEGRAL).

The high energy photons generated by the ^{24}Na source (at 1368.6 keV and 2754 keV), pass easily through the IBIS lateral shield and the source positioning is confirmed by the PICsIT shadowgram, shown in the left panel of Fig. 5, where the modulation of the photon flux, due to the projected hexagonal elements which constitute the SPI mask is clearly visible.

The image representing the whole upper hemisphere seen by IBIS, reconstructed using the event circle back-projection of down-scattered events, is shown in the right panel of Fig. 5. The source is clearly visible at the expected off axis angle ($\sim 40°$) in the direction of the negative Z axis, where the SPI instrument is located.

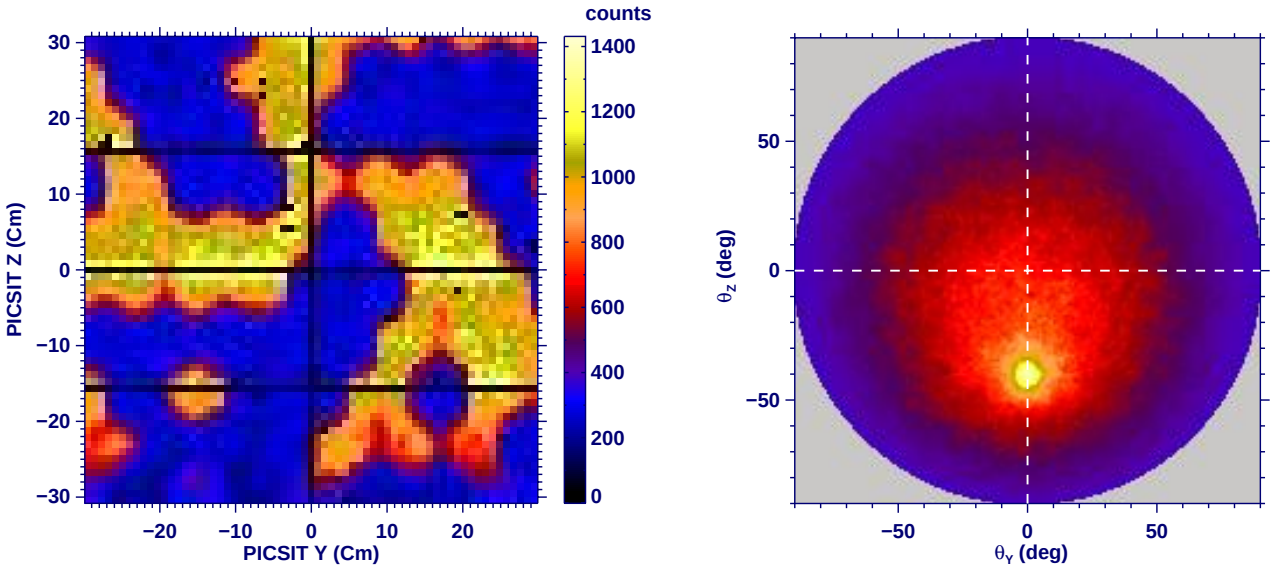

Figure 5. On the left, the PICsIT shadowgram generated by a ^{24}Na source located along the line of sight connecting the IBIS detector plane with the hexagonal SPI mask is shown. On the right, the upper hemisphere seen by IBIS reconstructed using simple Compton event circle back-projection (for down-scattered photons) is shown. The source is clearly visible at the expected off axis angle of $\sim 40°$, in the direction of the SPI instrument.

.

4.2. Directional accuracy

In order to verify the accuracy at which the direction of a source can be reconstructed using direct Compton imaging, it is necessary to analyze a Compton data set in which the coordinates of the radioactive source are known with very high precision. Since during INTEGRAL payload ground calibration the source position was not known with high accuracy, it is necessary to consider acquisitions where the source is placed within the IBIS

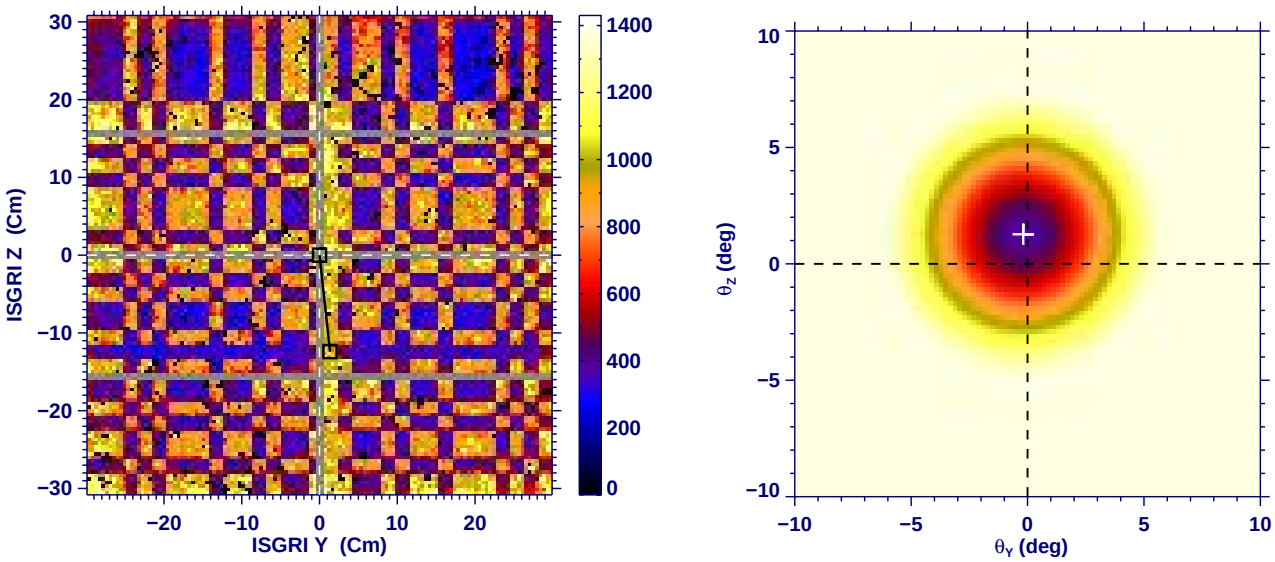

Figure 6. In the left panel, the ISGRI shadowgram generated by a ^{22}Na source placed few meters above the IBIS mask is shown. From the displacement of the projected mask central element with respect to the detector center (marked with squares), it is possible to estimate that the source is located at $\sim 1.3^\circ$ off axis angle. In the the right panel, the image reconstructed using the Compton kinematic is shown; the source reconsructed direction is consistent with the true source position within 0.1°.

coded field of view, so that the source coordinates can be obtained from the analysis of the shadow cast by the coded mask onto the detector plane.

Denoting with $D_{\rm I}$ the displacement of the projection of the mask central element onto the detector plane from the detector center, and with $D_{\rm M}$ the length of the mask segment that project this displacement (can be derived from the known mask pattern), the source off-axis angle ($\Theta_{\rm S}$) and its distance ($R_{\rm S}$) from the detector center can be obtained from:

$$\Theta_{\rm S} = arctan(D_{\rm M}/H_{\rm M}) \quad (4)$$

$$R_{\rm S} = \frac{\sqrt{H_{\rm M}^2 + D_{\rm M}^2}}{1 - D_{\rm M}/D_{\rm I}} \quad (5)$$

where $H_{\rm M}$ is the distance between the mask and the detector layer.

As example, the right panel of Fig. 6 shows the shadowgram of the ISGRI single events obtained when the detector was illuminated by a ^{22}Na source placed few meter above the IBIS mask but not in a perfect on-axis position. As evident from the illumination pattern, the mask central elements is projected at the detector coordinates $Y_{\rm C} = 1.35$ cm and $Z_{\rm C} = -12.4$ cm and this displacement is the projection of ~ 6.75 mask elements; considering that the real size of a mask element is 1.12 x 1.12 cm we then obtain $D_{\rm M} = 6.75 \cdot 1.12 = 7.56$ cm. Since the distance of the coded mask from the ISGRI layer is $H_{\rm M} = 320$ cm, we get, from Eq. 4 and 5, the following source coordinates:

$$\Theta_{\rm S} = 1.35^\circ$$
$$R_{\rm S} = 812 \text{ cm}$$

The source image, reconstructed from the Compton data of the considered acquisition, is shown in the right panel of Fig. 6. The source position, at $\theta_{\rm Y} = -0.18^\circ$ and $\theta_{\rm Z} = 1.27^\circ$, is consistent, within an error of the order of $\sim 0.1^\circ$, with the source coordinates computed from the mask shadowgram.

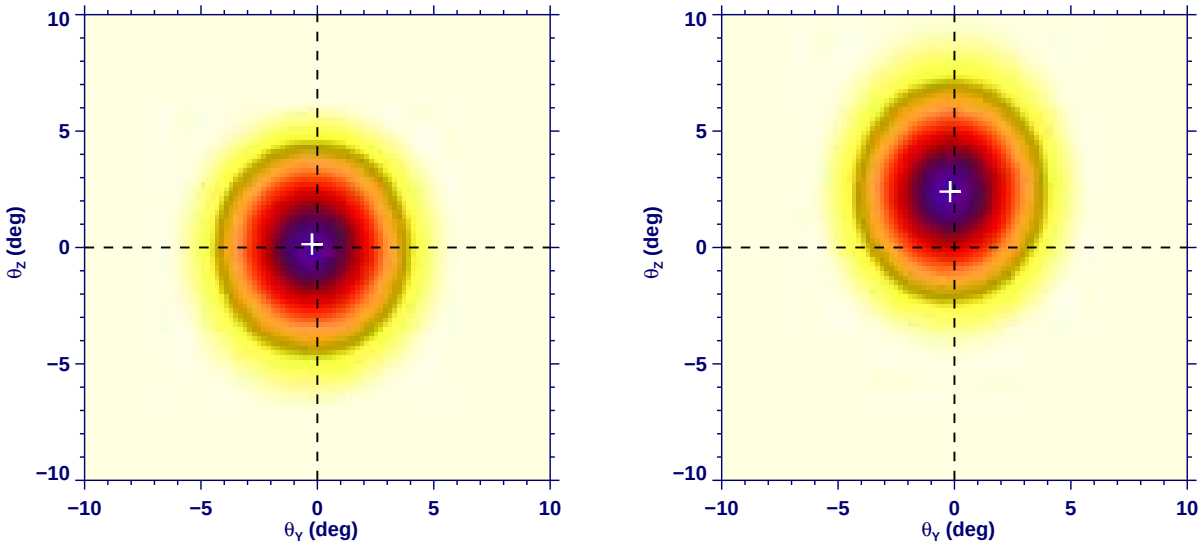

Figure 7. Compton sky images reconstructed, using the events in the ^{22}Na 511 keV line, without considering the source finite distance. The image on the left has been obtained selecting only Compton events associated to ISGRI pixels at Z> 15 cm while the image on the right has been obtained selecting the ISGRI pixels at Z< −15 cm. From the two reconstructed source positions it is possible to estimate the source distance.

Note that, in the reconstruction of images from the ground calibration Compton data, it is necessary to take into account the finite distance of the radioactive source from the detector, otherwise, since the source is seen by different regions of the detector at different angular positions an 'out of focus' effect would be generated.

For the ^{22}Na acquisition considered, the source position lies on the vertical intersecting the detector plane at coordinates Y_S=-1.5 cm and Z_S=19 cm so, if the finite source distance is not considered, the pixels in the positive Z axis reconstruct the source in an almost on-axis position while the pixels in the negative Z axis reconstruct the source at an off-axis angle higher than the one measured from the detector center. This effect is shown in Fig. 7, where the image on the left has been obtained by selecting only events associated to the ISGRI pixels with the Z coordinate > 15 cm, while the image on the right has been obtained selecting only the events associated to ISGRI pixels with the Z coordinate < -15 cm.

This example, beside confirming the good directional accuracy obtainable from the Compton imaging, shows also that, when the source distance is unknown, subdividing the Compton events according to their interaction position in different regions of the detector plane, it is possible to obtain two or more images that, combined in a sort of stereoscopic way, allow to determine the source position.

5. MASK IMAGING

When the source is in within the IBIS coded field of view, mask imaging and event selections based on the Compton kinematics can be combined in order to obtain skymaps with high spatial resolution and low background.

A sky image can be in fact obtained by convolving the shadowgram associated to the ISGRI part of the Compton events with the IBIS mask pattern and its S/N ratio optimized by ARM selections, using the a priori known source position.

Assuming that the ARM distribution of source photons can be approximated by a gaussian line ($\sigma_{\rm ARM}$), and that the distribution of background events can be approximated, in a region close to the origin, by a straight line, the optimum S/N ratio can be computed analytically and its maximum value is obtained, in case of background dominated source, by selecting only the events within $|ARM| < 1.4 \cdot \sigma_{\rm ARM}$. Using this selection we retain $\sim 84\%$ of the events in the gaussian line, however the real efficiency is further reduced by the fact that most of the multiple scattered Compton events, which form a long tail on the right side of the line, will also be discarded.

The event selection can be further optimized using ARM ranges which take into account the variations of the angular resolution as function of the energy and of the Compton scattering angle, as shown in Fig. 3.

Note that up-scattered photons (that is photons scattered by PICsIT), interact with the ISGRI detector in positions uncorrelated with the coded mask pattern, so they behave as background events. In order to generate a skymap using the up-scattered photons, it is necessary to deconvolve the shadowgram of the PICsIT part of the Compton events. However, considering that the size of one PICsIT pixel is 4 times the size of one ISGRI pixel, the skymaps obtainable in this way have worst angular resolution and considering also that up-scattered events are less numerous than the down-scattered events, in such images the S/N would be much poorer with respect to the images obtainable from the deconvolution of the shadowgrams of the ISGRI part of the Compton events.

Whit respect to 'Compton' direct imaging, 'Mask imaging' produces images with a much better angular resolution and S/N ratio; moreover these images are already background subtracted. A main drawback of this method is however that the images generated are affected by the presence of random coincidences.

In fact, source 'single' event detected by ISGRI in random coincidence with PICsIT background events generate 'fake Compton' events that contribute to the image in exactly the same way as true source 'Compton' events but, of course, at a fake energy. So in the Compton skymaps obtained by shadowgram deconvolution, events generated by random coincidences reproduce a scaled replica, shifted at higher energies, of the skymap obtainable from the 'single' events.

This is a main problem in particular for the astronomical sources. In fact due to the fast decrease with energy of the photon source spectra and of the detector efficiency, Compton events will be always much less numerous that 'single' events, so, even is the probability of random coincidence is low, the total number of 'fake' events can be much higher than the number of 'true' Compton events. Random coincidences must be then subtracted very accurately to avoid fake source detections in the Compton energy range.

Note that images obtained using only the Compton kinematics are not sensitive to this kind of contamination since the Compton angles of the 'fake' events are randomly distributed, generating then only an increase of the average background level.

6. IN-FLIGHT COMPTON DATA

6.1. The on-Board Calibration Unit

In order to verify wether the in-flight imaging performances of the IBIS Compton data are degraded with respect to the performances measured during the on-ground calibration, we have analyzed the data generated by the IBIS on-board Calibration Unit[8] (CU), that consists of a ^{22}Na radioactive source (activity = 0.4 μCi at launch date) placed at detector coordinates $(Y, Z)_{\rm CU}$ = (-51.2 cm, 0 cm), 220 cm above the ISGRI detection plane.

The CU is oriented so to illuminate the whole detector layer and a tagging system is implemented in order to detect one of the two 511 keV photons emitted during the radioactive decay of the ^{22}Na source. Any energy deposit in PICsIT or ISGRI which is detected in coincidence with a calibration strobe (width = 2μs) is flagged, and regarded as a calibration event. Compton events are then subdivided into two categories, depending whether they are detected in coincidence with a calibration strobe or not.

In the right panel of Fig. 8, it is shown the image reconstructed by event circle back-projection, obtained selecting only the Compton events in coincidence with the calibration strobe. The 'event circles' have been generated by the intersection of the Compton cones with the surface of a sphere having the radius equal to the known distance of the CU from the detector center. The calibration source is clearly visible, reconstructed at 14° off-axis angle in the direction of the negative Y axis. The reconstructed angular position of the CU, agrees very well with its nominal position.

In the right panel of Fig. 8, the CU in-flight ARM distribution (for down-scattered photons) is shown. The line width is consistent with the value measured on-ground, demonstrating then that the in-flight performances of the Compton data are not significantly degraded.

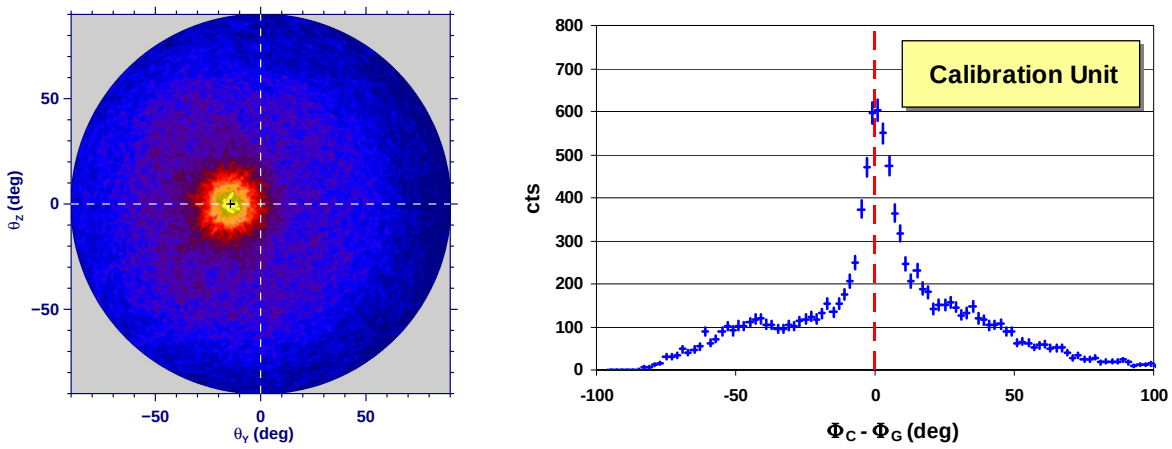

Figure 8. Left panel: In-flight Compton skymap obtained selecting events in coincidence with the Calibration Unit strobe. The calibration source is clearly visible at $\sim 14^{\circ}$ off axis angle. Right panel: the ARM distribution obtained selecting Compton events in the 511 keV line in coincidence with Calibration Unit strobe. The line width is consistent with the ground measurements.

6.2. Crab observation

In order to determine the capabilities of IBIS Compton data from the astrophysical point of view, we have analyzed the data relative to the Crab observations.

The skymap obtained as result of the deconvolution of the ISGRI shadowgram of Compton data from a 56 ksec Crab on-axis pointing, is shown on the left panel of Fig. 9. In this image the Crab is clearly detected, with a very good S/N ratio and with the angular resolution expected. However, after careful estimation and subtraction of the contribute of random coincidences, we obtain a cleaned skymap, shown on the right panel, where the Crab is no more visible.[6]

We get similar results after applying ARM selections in order to improve the image S/N ratio. Although with ARM selections the background count rate is greatly reduced (up to 70%), no evidence of the Crab source is found in the skymaps cleaned from the random coincidences. From the selected data set we can only derive an upper limit for the Compton count rate generated by the Crab in the whole energy range of the order of $\sim$ 0.05 cts/sec.

To perform a deeper analysis of the Crab data, we have generated two ARM distributions: the first one selecting only events associated to the ISGRI pixel illuminated by the Crab through the open elements of the IBIS coded mask (this distribution contains Crab plus background events) and the second one, by selecting only events associated to ISGRI pixels not illuminated by the Crab (this distribution contains only background events). From the difference between these two distributions we obtained the background subtracted ARM distribution of the Crab events. The results are shown in Fig. 10 in two energy ranges.

As evident, in the background subtracted ARM distributions of the Compton data there is no evidence at all of the narrow gaussian line at the origin that should be associated to true Compton events, confirming that the Crab image obtained by shadowgram deconvolution, is entirely due to the random coincidences between Crab ISGRI 'single' events and PICsIT background events.

7. CONCLUSIONS

We analyzed IBIS Compton data acquired during the INTEGRAL payload calibration and during in-flight operations in order to determine its scientific capabilities.

We showed that in the analysis of Compton data, in addition to the usual background subtraction, it is highly important to perform an accurate subtraction of the random coincidences to avoid false source detections.

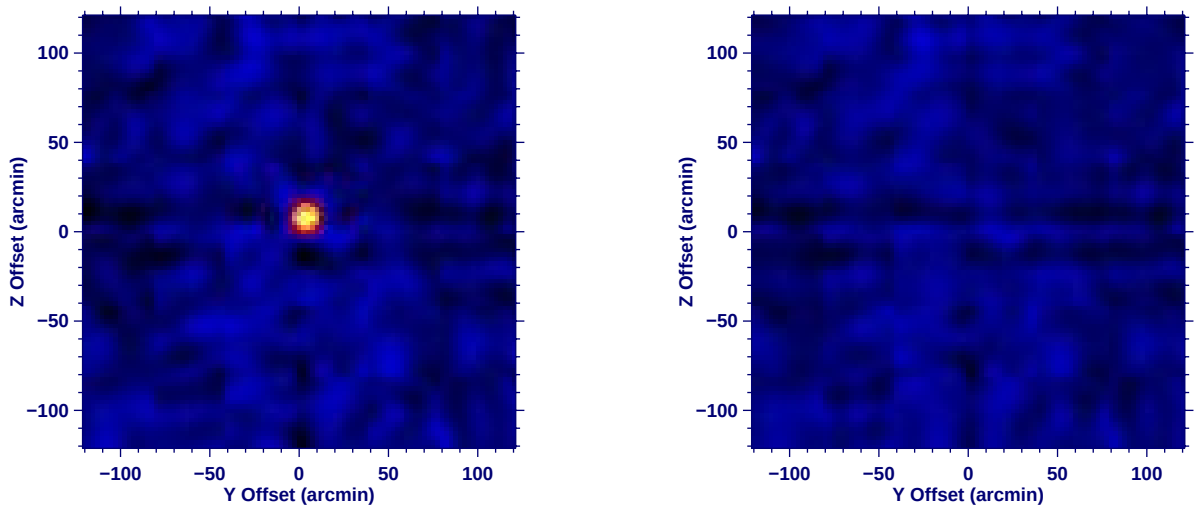

Figure 9. Skymaps obtained from 56 ksec sec of IBIS Compton data of a Crab pointing. The image on the left is the result of the convolution of the shadowgram of the ISGRI part of the Compton events with the mask pattern. On the right, the image obtained after the subtraction of the random coincidences is shown.

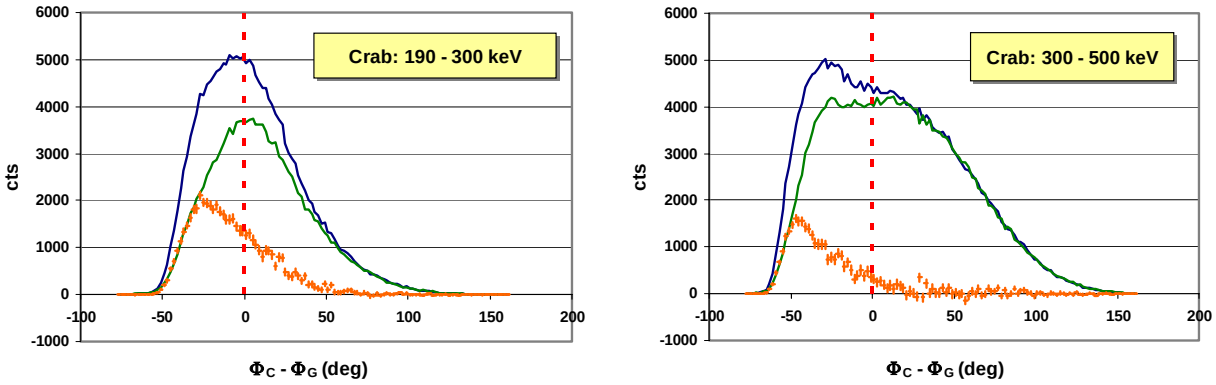

Figure 10. ARM distributions obtained from the Compton data of a 56 ksec Crab observation. In each panel, the two upper curves are the distributions associated to ISGRI pixels illuminated and not illuminated by the Crab through the coded mask. Their difference (crosses) is also shown. The fact that there is no evidence of a gaussian line at the origin, indicates that the totality of the Crab events in the Compton data are due to random coincidences.

We obtained skymaps from the Compton data using Compton kinematics and found that the average angular resolution obtainable is $\sim 10^\circ$ FWHM with variations as function of photon energy and scattering angle, and that the source direction can be reconstructed in a wide field of view and with an error of $\sim 0.1^\circ$.

We have checked the Compton in-flight performance by selecting Compton events in coincidence with the Calibration Unit strobe and found no significant degradation with respect to the on-ground measurents.

We have then generated, by mask deconvolution, images from Compton data of the Crab on-axis observation and found no evidence of the source after the subtraction of random coincidences. This result as been confirmed by the analysis of the background subtracted ARM distribution of the Crab data, where no evidence at all of the typical signature of true Compton events is visible.

From the statistics of the considered data set ($\sim$ 56 ksec) we have derived an upper limits of 0.05 cts/sec for the total Compton count rate that can be associated to Crab emission in the whole energy range.

Several reasons contribute to the poor sensitivity of the Compton data:

- it is not possible to distinguish, from the time of flight, events generated by down-scattered from up-scattered photons.
- due to the jitter on the event arrival times of ISGRI detector, the Compton coincidence time window must be wider than the instrumental time resolution. This fact, together to the high background count rates, generate numerous fake Compton events which can give origin to fake source detections.
- due to the low probability of photoelectric interaction in PICsIT, a quite high fraction of the Compton events are generated by multiple scattered photons. Since the scattering angle of these events is wrongly estimated, most of them are discarded when ARM selection is applied.
- the angular resolution obtainable in the ARM distribution ($\sim 10^\circ$ FWHM) limits the possibility to reduce the background applying very narrow selections without discarding also source events.

From the performed analysis, it is clear that the astrophysical results obtainable from the IBIS Compton data are severely limited by photon statistics and by an extremely low signal to noise ratio. Considering that it was not possible to detect the Crab, using different methods and selections, in 56 ksec of Compton data, the 3σ sensitivity of this mode is surely higher than 240 mCrab in 10^6 sec, without taking into account possible systematic errors in the subtraction of random coincidences, that could easily lead to fake source detections.

ACKNOWLEDGMENTS

We wish to thank T. Mineo for the useful comments and suggestions.

REFERENCES

1. P. Ubertini; F. Lebrun; G. Di Cocco, et al., A&A 411, L131, 2003
2. F. Lebrun, J. P. Leray, P. Lavocat, et al., A&A 411, L141, 2003.
3. G. Di Cocco, E. Caroli, E. Celesti, et al., A&A 411, L189, 2003.
4. M. Forot, P. David, P. Laurent, et al., "Study of the Crab pulsar wih the IBIS/Compton mode", in press: Proceed. of 5th INTEGRAL Workshop (Munich, Feb 2004), ESA SP-Series, 2004.
5. A. Segreto, "IBIS Compton mode: analysis of the random coincidences", in press: Proceed. of 5th INTEGRAL Workshop (Munich, Feb 2004), ESA SP-Series, 2004.
6. A. Segreto, "IBIS Compton mode: subtraction of the random coincidences", in press: Proceed. of 5th INTEGRAL Workshop (Munich, Feb 2004), ESA SP-Series, 2004.
7. V. Schönfelder, H. Aarts, K. Bennett, et al., ApJ suppl., vol 86, p657, 1993
8. A. J. Bird, A. Bazzano, C. Ferguson, et al., A&A 411, L197, 2003